GEOLOGY | THE GEOLOGICAL SOCIETY OF AMERICA®

https://doi.org/10.1130/G51796.1

Manuscript received 12 October 2023
Revised manuscript received 28 December 2023
Manuscript accepted 18 January 2024

Published online 6 February 2024

Intersection between tectonic faults and magmatic systems promotes swarms with large-magnitude earthquakes around the Tengchong volcanic field, southeastern Tibetan Plateau

Min Liu[1,2], Yen Joe Tan[1,*], Xinglin Lei[3], Hongyi Li[2], Yunpeng Zhang[4], and Weitao Wang[4]

[1]Earth and Environmental Sciences Programme, Faculty of Science, The Chinese University of Hong Kong, Hong Kong S.A.R., China, 999077

[2]Key Laboratory of Intraplate Volcanoes and Earthquakes, Ministry of Education, China University of Geosciences (Beijing), Beijing, China, 100083

[3]National Institute of Advanced Industrial Science and Technology, Tsukuba, Japan, 305-8567

[4]Institute of Geophysics, China Earthquake Administration, Beijing, China, 100036

ABSTRACT

Volcanic regions commonly host swarms comprising small to moderate-sized earthquakes while tectonic faults host mostly mainshock-aftershock sequences that can include very large earthquakes. In the southeastern Tibetan Plateau, large tectonic faults formed by the collision between the Indian and Eurasian plates intersect with the intraplate Tengchong volcanic field, and the seismic behavior of such an environment remains unclear. Here, we built a deep-learning-based high-precision earthquake catalog for the Tengchong volcanic field and found that (1) ~59% of the seismicity occurred as swarms but on faults aligned with the regional tectonic stress field; (2) all swarms contained fluid-diffusion-like migration fronts, with some occurring where high CO_2 emissions have been detected; and (3) a year-long swarm, including two M_L 5.2 earthquakes within two months, revealed complex fluid-fault interaction. Combined with the historical occurrences of M >6 earthquake swarms around the Tengchong volcanic field, our observations suggest potential increased likelihood of swarms with large-magnitude earthquakes where large tectonic faults and magmatic systems intersect.

INTRODUCTION

Earthquake swarms, which are earthquake sequences that lack a distinct mainshock (Mogi, 1963), are common in volcanic regions, where they are commonly inferred to manifest underlying magmatic or fluid processes (Wilding et al., 2023). Due to material and stress field heterogeneity as well as the lack of large faults (Hill, 1977), volcanic swarms are dominantly composed of M_W <4.5 events (Cox, 2016), though occasionally volcanic swarms associated with eruptions or caldera collapses can include large earthquakes ($5.0 < M_W < 7.0$; Hildreth and Fierstein, 2012; Patrick et al., 2020). In comparison, tectonic faults in relatively homogeneous regions under uniform stress fields tend to accommodate mainshock-aftershock sequences in which the seismicity rate and probability of large events decrease with time after the mainshock (Mogi, 1963). While earthquake swarms sometimes occur on tectonic faults because of underlying fluid diffusion or aseismic slip (Vidale and Shearer, 2006), they are less common than in volcanic regions. Globally, there are numerous regions where large tectonic faults intersect with volcanic systems (e.g., Mount Aso in Japan). However, how the interaction between magmatic systems and tectonic faults affects the seismic behavior and hazard of such regions remains unclear.

The collision between the Indian and Eurasian plates caused the rise and eastward extrusion of the Tibetan Plateau (Fig. 1A). The complex deformation created a series of large-scale active faults in the southeastern margin of the Tibetan Plateau (Tapponnier et al., 1982), such as the Longmenshan, Red River, and Nujiang fault systems, which are responsible for the majority of earthquake activity in China and have hosted 83 M >6.5 earthquakes since 1327 (Li et al., 2023). The southeastern Tibetan Plateau intersects with the Tengchong volcanic field, which is an intraplate volcanic system that consists of 68 volcanoes (Fig. 1A; Duan et al., 2019). While the volcanic field has been in quiescence since its last eruption in 1609, it still exhibits signs of active magmatic activity, such as large amounts of CO_2 emissions (Chen et al., 2012), high surface heat flow (Hu et al., 2000), and occasional geysers (Shangguan et al., 2005). The fault structures around the Tengchong volcanic field are complex but predominantly accommodate right-lateral strike-slip movement, with the ~450-km-long Nujiang fault surrounded by dense secondary faults (Deng et al., 2003), including the Dayingjiang and Longchuanjiang faults, which cut through the volcanic field (Fig. 1A). The Tengchong volcanic field and its adjacent areas have hosted intense seismic activity, including two M 6.5 earthquakes in 1512 and 1577 in the central volcanic field, a swarm of seven M >6.0 earthquakes from 1929 to 1933 in the northern volcanic field, and two M 7.2 earthquakes within two hours in 1976 in the southeastern volcanic field (Fig. 1A). Therefore, the Tengchong volcanic field serves as a unique laboratory to probe the interaction between magmatic systems and large-scale tectonic faults. In this study, we processed continuous seismic data from 2009 to 2022 and built a high-resolution earthquake catalog for the Tengchong volcanic field to characterize the seismicity and analyze its underlying driver.

CHARACTERIZATION OF SEISMICITY IN THE TENGCHONG VOLCANIC FIELD

We adopted a deep-learning-based workflow to develop a 13-yr earthquake catalog including 10,078 events that were precisely located using a

Yen Joe Tan https://orcid.org/0000-0001-6377-7886
*yjtan@cuhk.edu.hk

CITATION: Liu, M., et al., 2024, Intersection between tectonic faults and magmatic systems promotes swarms with large-magnitude earthquakes around the Tengchong volcanic field, southeastern Tibetan Plateau: Geology, v. 52, p. 302–307, https://doi.org/10.1130/G51796.1

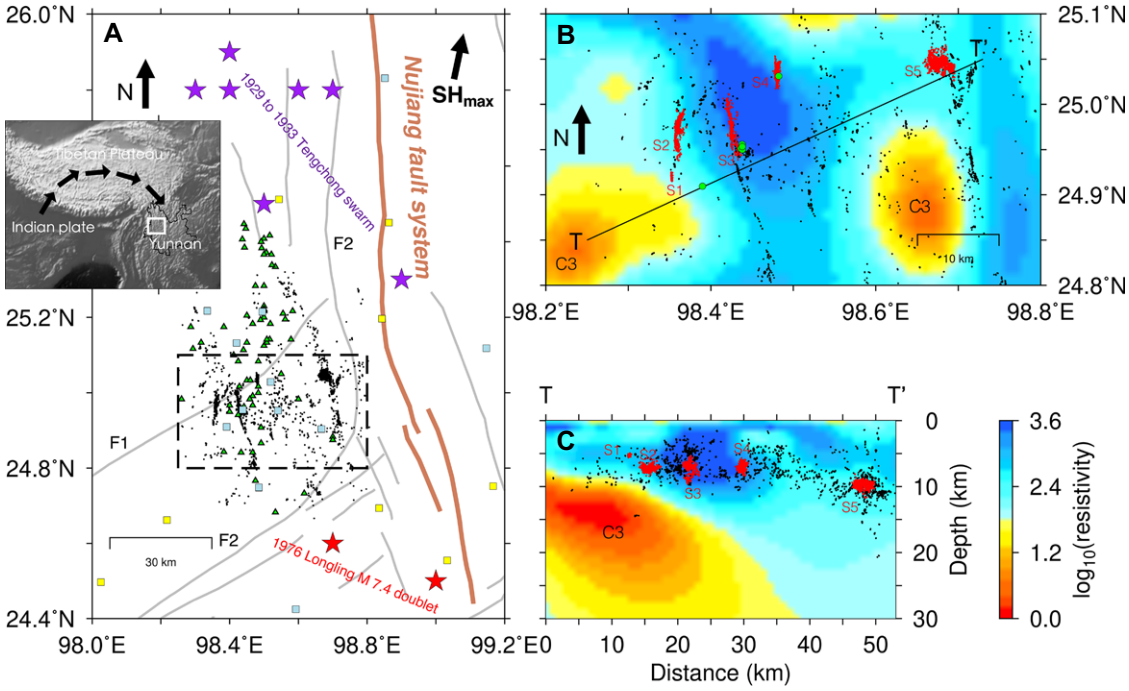

Figure 1. (A) Map view of study area, Tengchong volcanic field, southeastern Tibetan Plateau. Squares represent permanent (blue) and temporary (yellow) seismic stations. Green triangles indicate the location of volcanic cones (Duan et al., 2019). Red stars show the epicenters of the 1976 M 7.4 doublet. Purple stars show the epicenters of the seven M >6 earthquakes in the 1929–1933 swarm. Black dots show our located earthquakes from 2009 to 2022. F1 and F2 mark the Dayingjiang and Longchuanjiang faults, respectively. Arrow indicates the greatest principal stress orientation (SH_{max}) of ~N10°E. Inset shows regional tectonic movement (black arrows) and our study area (white box). (B) Zoom-in of our study area marked in A by the black dashed rectangle. Red dots represent the five identified swarms (S1–S5). Green dots represent CO_2 monitoring sites (Chen et al., 2012). Black line marks the profile TT′ shown in C. C3 indicates the inferred magma chamber from three-dimensional magnetotelluric tomography (Ye et al., 2018). (C) Cross-section along profile TT′ shown in B.

waveform cross-correlation-based method (Text S1–S4 in the Supplemental Material[1]; Liu et al., 2023). The earthquakes occurred primarily in the southern Tengchong volcanic field and revealed multiple previously unmapped faults that mostly strike north-northwest or near north (Fig. 1). The earthquakes are predominantly located in the upper crust, with the eastern events located deeper (7–15 km depth) than the western events (2–10 km depth; Fig. 1C). We further identified earthquake swarms with at least 100 events (Figs. 1B and 1C; Fig. S1 in the Supplemental Material) using the DBSCAN algorithm (Ester et al., 1996) and manual inspections (Text S5). In total, we identified five swarms comprising 5905 events, which represent ~59% of the newly developed catalog. These swarms are significantly different from mainshock-aftershock sequences where the largest event occurs toward the beginning of the sequence (Fig. S1). The spatial extents of the swarms are also larger than the expected rupture dimensions of the largest events. For instance, swarms 2 and 4 extended 4–6 km laterally (Figs. 2B and 2F), while the expected dimensions of their largest events (M_L 4.5 and 4.6) are <~1.5 km (Wells and Coppersmith, 1994; Text S6). The five swarms follow similar spatiotemporal evolution, initiating at a point before migrating outward over days to months (Figs. S1 and S2). In addition, all five swarms exhibit migration fronts that can be fitted reasonably well using the fluid diffusion model (Figs. 2 and 3; Fig. S3; Shapiro et al., 1997). Meanwhile, some swarms exhibit clear back fronts (swarms 2, 3, and 5; Fig. S3; Parotidis et al., 2004). Swarms 1–4 generally delineate simple planar faults that are 1–6 km long, whereas swarm 5 outlines a complex fault network (Fig. 1B).

Swarm 5 lasted approximately one year with a complex evolution that can be divided into four phases by three main events: M_L 4.7 on 31 May, M_L 5.2 on 20 June, and M_L 5.2 on 7 August 2011 (Fig. S1). Phase 1 began on 17 November 2010 with some small events (M_L <3.0) at a depth of ~9.3 km (Figs. 3A and 3B). The seismicity then migrated ~1 km northwest and down to ~9.7 km depth, delineating a southwest-dipping fault plane (Figs. 3A and 3B). The late evolution of phase 1 exhibits a clear migration front, which can be modeled by a diffusivity of 0.02 m^2/s (Fig. 3C; Shapiro et al., 1997). Subsequently, an M_L 4.7 event occurred near where the downward migration of phase 1 terminated (Figs. 3A and 3B; Fig. S4), initiating phase 2 on 31 May 2011. The seismicity then migrated ~1.2 km northeast and down to ~10.3 km depth, overall delineating a conjugate structure at depth (Figs. 3D and 3E). The northeasternmost events are characterized by an isolated cluster of events (cluster 1) that started at a point before migrating outward in all directions (Figs. 3D and 3E).

On 20 June 2011, an M_L 5.2 earthquake nucleated near the base of the conjugate structure and initiated phase 3 (Fig. 3E). Subsequent events rapidly migrated northwest, delineating a downward-extending ring fault (Figs. 3F and 3G). The focal mechanisms of nine M_L >2.5 earthquakes (Text S7) that occurred within the ring structure exhibit rotated nodal planes (Fig. S5) consistent with the structure's complex geometry. In addition, cluster 1 subsequently extended farther in the southwest direction with a diffusive migration front (Fig. S6). Meanwhile, a new isolated cluster of events (cluster 2) occurred ~2 km southeast of the M_L 5.2 earthquake, outlining an ~1-km-long, northwest-dipping fault plane (Fig. 3F; Fig. S7a). Cluster 2 also exhibited a diffusive migration front with a diffusivity of 0.2 m^2/s (Fig. S7b). Less than two months later on 7 August 2011, another M_L 5.2 earthquake nucleated near the edge of cluster 2 and initiated phase 4 (Fig. 3F; Fig. S7a). In phase 4, early events delineated an ~2-km-long, northwest-trending fault plane (Figs. 3H and 3I). Five days later, the seismicity reactivated the western part of the complex fault network of phase 3, especially the downward-extending ring fault (Fig. 3H).

DISCUSSION AND CONCLUSIONS

Seismogenesis of Swarms in the Tengchong Volcanic Field

Fluid and aseismic slip are commonly inferred to be the main drivers of swarms (Vidale and Shearer, 2006). In our study, each identified

[1]Supplemental Material. Seismic data processing procedure and high-resolution earthquake catalog. Please visit https://doi.org/10.1130/GEOL.S.25057634 to access the supplemental material; contact editing@geosociety.org with any questions.

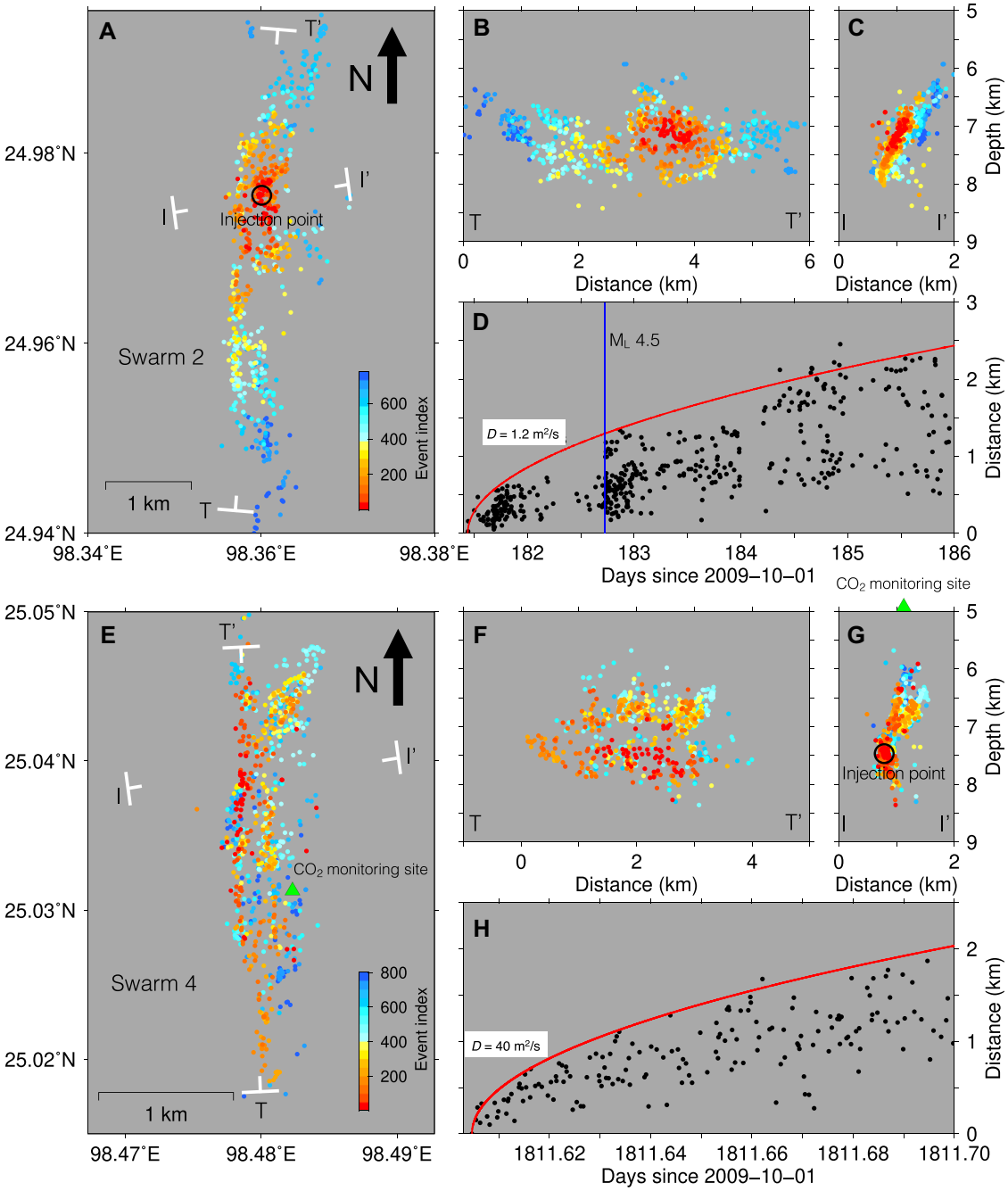

Figure 2. Spatiotemporal evolution of earthquake swarms 2 and 4 (see Fig. 1). (A) Map view of swarm 2 with color indicating event index, which was sorted by earthquake origin time. White bars show the two profiles TT′ and II′ exhibited in (B) and (C), respectively. (D) Distance from the inferred fluid injection point with time. Red solid curve represents the best-fit fluid diffusion model (Shapiro et al., 1997): $r = \sqrt{4\pi Dt}$, where r is the distance of an earthquake from the injection point, t is time, and D is diffusivity. (E–H) Similar to A–D, but for swarm 4. Green triangles in E and G mark the CO_2 monitoring site (Chen et al., 2012).

swarm exhibits at least one migration front that can be well fitted by the fluid diffusion model, with diffusivities ranging from 0.01 to 40 m^2/s (Figs. 2 and 3; Fig. S3). Swarms 2, 3, and 5 also exhibit clear back fronts (Fig. S3), which have been inferred to represent the termination of fluid injection (Parotidis et al., 2004). In addition, previous studies have found: (1) large volumes of CO_2 emission in the Tengchong volcanic field including at the surface above swarms 3 and 4 (Figs. 1B and 2G; Chen et al., 2012); (2) widespread hydrothermal systems in the Tengchong volcanic field (Guo et al., 2017); and (3) tidal modulation of seismicity in the area around swarm 5 in the two years before the first M_L 5.2 earthquake (Peng et al., 2021). These observations suggest that these swarms were likely driven by fluids, which decreased the effective normal stress on pre-existing faults.

In situ experiment (Guglielmi et al., 2015) and field seismic observation (De Barros et al., 2020) have indicated that fluid diffusion and aseismic slip may be imbricated in swarms, where fluid pressure first induces aseismic slip, which in turn triggers seismicity through stress perturbation. We cannot exclude the possibility that similar processes are at play for the swarms in the Tengchong volcanic field but note that even in such a scenario, fluids would remain the fundamental underlying driver of the swarms in the volcanic field. In addition, we observe that some linear migration fronts were embedded in the evolution of swarms 2 (Fig. 2D) and 5 (Fig. 3C; Fig. S7b), which may be associated with stress transfer triggering or the manifestation of aseismic slip (De Barros et al., 2020). Besides, the 40 m^2/s apparent diffusivity of swarm 4 is higher than the general diffusivities of 0.01–10 m^2/s in the crust (Scholz, 2019) but is lower than that of some fluid-driven swarms in geothermal regions, such as the 1997 Umbria-Marche (central Italy) sequence (22–90 m^2/s; Antonioli et al., 2005) and the 2018–2020 Noto Peninsula (Japan) sequence (~200 m^2/s; Amezawa et al., 2023). The high apparent diffusivity may be explained by the presence of pressurized fluids at depth and the high permeability of fault zones or simply reflect the

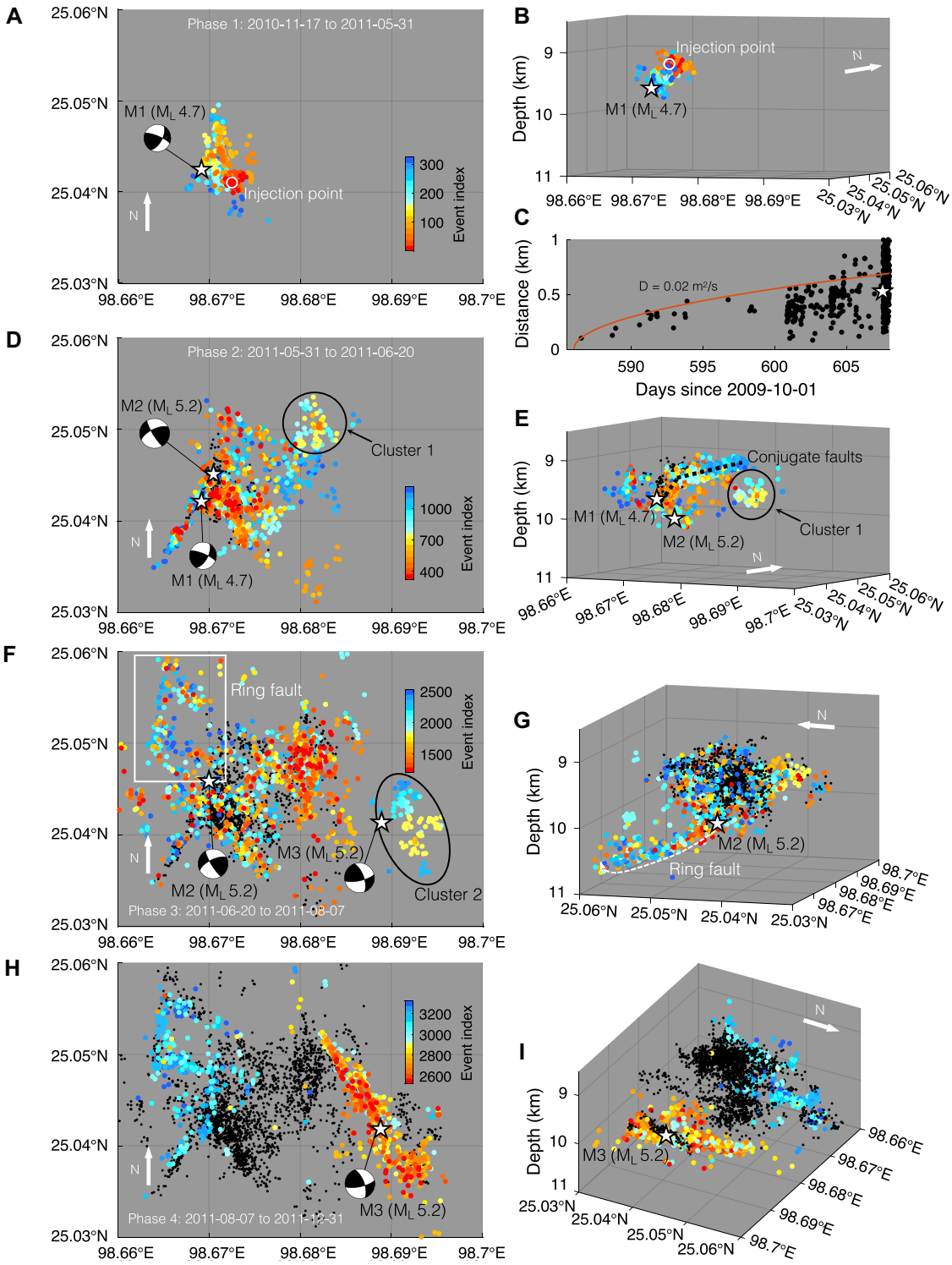

Figure 3. Spatiotemporal evolution of earthquake swarm 5 (see Fig. 1), which is divided into four phases by three main events (M1–M3; white stars). (A) Map view of earthquakes that occurred during phase 1 with color indicating event index. Beach ball shows focal mechanism of main event. (B) Similar to A, but in three-dimensional (3-D) view. (C) Earthquake distance (black dots) from the inferred fluid injection point with time. Red solid curve represents the best-fit fluid diffusion model with a diffusivity D = 0.02 m²/s (Shapiro et al., 1997). (D) Similar to A, but for phase 2. Black dots represent earthquakes that occurred before the current phase. (E) Similar to D, but in 3-D view. (F) Similar to A, but for phase 3. White rectangle indicates a ring fault exhibited in 3-D view in (G). (H, I) Similar to F and G, but for phase 4.

complex interaction of multiple mechanisms. Besides, recent numerical modeling suggested that actual hydraulic diffusivity may be higher than that inferred from seismic migration fronts due to non-instantaneous earthquake nucleation (Kim and Avouac, 2023). Nevertheless, the overall evolution of seismicity at the Tengchong volcanic field still points to the significant influence of fluids.

Interaction between Tectonic Faults and Magmatic Systems

Seismic behavior of volcanic regions significantly differs from that of tectonic fault systems. Volcanic seismicity commonly occurs as swarms consisting of small to moderate events (Cox, 2016), while tectonic faults mostly accommodate mainshock-aftershock sequences that can include very large earthquakes (Mogi, 1963). While previous studies have identified swarms occurring on tectonic faults, tectonic swarms are less common than volcanic swarms (e.g., Ross and Cochran, 2021). At the Tengchong volcanic field, we find that even though the seismicity delineates fault strikes that align with previously mapped large tectonic faults and the regional tectonic stress field (Fig. 1A; Fig. S8), at least ~59% of the earthquakes occurred as swarms.

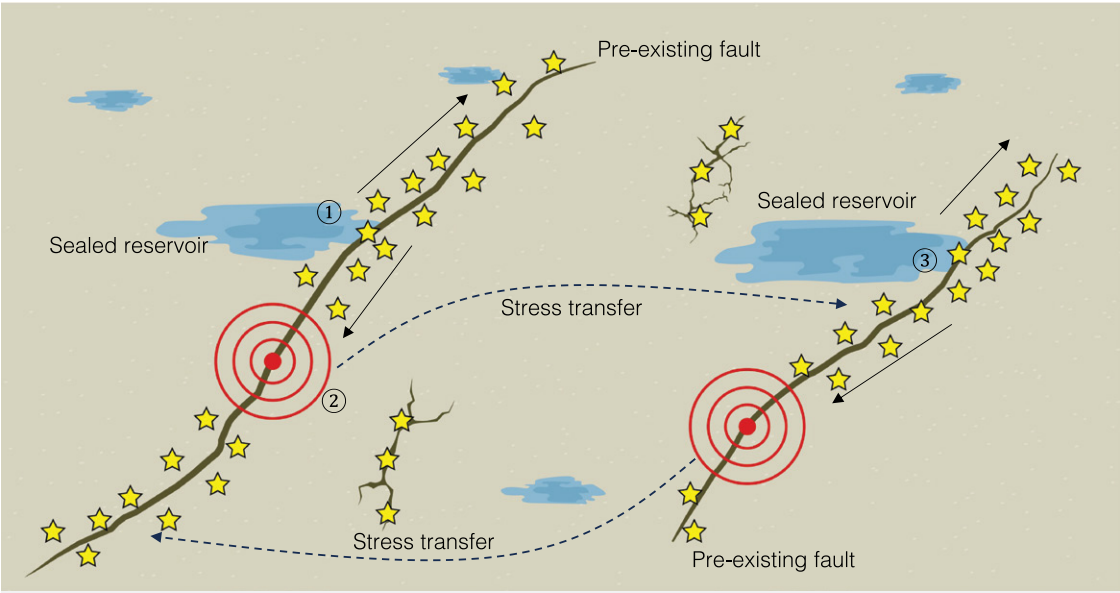

① Fluid diffusion from connected reservoir into pre-existing fault zone (black arrows) can trigger earthquake swarm (yellow stars) which can include large earthquake (red circles) if fault (black lines) is large.
② Stress triggering can further activate surrounding fault systems.
③ Static and dynamic stress due to earthquakes can break previously sealed reservoir(s), with resulting fluid diffusion triggering more seismicity and further extending earthquake sequence.

Figure 4. Cartoon illustrating the interaction between fluids and faults at the Tengchong volcanic field.

Therefore, these swarms likely reflect the reactivation of pre-existing tectonic faults by fluids that are prevalent due to the presence of an underlying magmatic system (Fig. 1C; Brenguier et al., 2014; Ye et al., 2018).

The interaction between pre-existing tectonic faults and hydrothermal or magmatic fluids is illustrated by the complex evolution of swarm 5, which included two M_L 5.2 earthquakes with different rupture behaviors (Fig. 3; Fig. S1). Swarm 5 initiated in a local area and then migrated outward with a clear migration front that can be modeled with fluid diffusion, with the seismicity delineating a planar structure (Fig. 3). This suggests that a pre-existing fault zone was activated by fluid diffusion possibly from a connected reservoir. An M_L 4.7 earthquake followed by the first M_L 5.2 earthquake subsequently nucleated at the edge of preceding seismicity (Fig. 3E), activating a downward-extending ring fault that does not align with the regional stress field and hence could be a product of a local stress field related to pressurized fluid reservoirs (Figs. 3F and 3G). Such complex faulting is rare in typical mainshock-aftershock sequences but has been observed during fluid-driven swarms because permeability structure could be similarly complex (Bense and Person, 2006; Shelly et al., 2013). These observations also reflect the "fault valving" mechanism in which earthquake faulting can dramatically increase permeability and enable fluids to flow farther (Sibson, 1981). Besides, the M_L 5.2 earthquake triggered an isolated sub-swarm (cluster 2) that exhibited a diffusive migration front (Fig. 3F; Fig. S7). This suggests the M_L 5.2 earthquake might have broken the seal of another reservoir, which activated another fluid-driven earthquake sequence. A second M_L 5.2 earthquake eventually nucleated near the edge of cluster 2 and activated a simple ~2-km-long planar fault (Figs. 3H and 3I) that is well-aligned with the typical tectonic earthquakes. The seismicity five days after this second M_L 5.2 earthquake in turn reactivated the ring fault (Fig. 3H). Geological investigation has highlighted a similar role of fluid-faulting interaction during the reactivation of interconnected fault networks (Dempsey et al., 2014). Therefore, the evolution of swarm 5 further illustrates how the interaction between fluid diffusion and stress triggering when large faults are present can result in multiple isolated fault structures and fluid reservoirs being activated in a complex extended sequence that includes multiple large earthquakes (Fig. 4).

The underlying interaction mode between hydrothermal or magmatic fluids and tectonic faults at the Tengchong volcanic field revealed by recent seismicity may explain the numerous historical large-magnitude swarms that occurred in the vicinity of the volcanic field, such as the seven M >6.0 earthquakes during the 1929–1933 Tengchong swarm and the 1976 Longling M_W 7.2 doublet (Fig. 1A). Thus, our observations suggest that interaction between tectonic faults and magmatic systems can promote the occurrence of large-magnitude swarms. Similar environments can be found globally, such as at the Coso volcanic field in the United States, Mount Aso in Japan, and the Andean Cordillera in South America. Therefore, further study of fluid-fault interaction in these regions is critical to improve our ability to manage future earthquake hazards.

ACKNOWLEDGMENTS

The authors thank editor Robert Holdsworth, Krittanon Sirorattanakul, and two anonymous reviewers for their comments and suggestions. This work is supported by the National Natural Science Foundation of China (grant 42122060), the Hong Kong Research Grant Council Early Career Scheme (grant 24305521), the Croucher Tak Wah Mak Innovation Award, and the Chinese Fundamental Research Funds for the Central Universities (grant 2652023001).

REFERENCES CITED

Amezawa, Y., Hiramatsu, Y., Miyakawa, A., Imanishi, K., and Otsubo, M., 2023, Long-living earthquake swarm and intermittent seismicity in the northeastern tip of the Noto peninsula, Japan: Geophysical Research Letters, v. 50, https://doi.org/10.1029/2022GL102670.

Antonioli, A., Piccinini, D., Chiaraluce, L., and Cocco, M., 2005, Fluid flow and seismicity pattern: Evidence from the 1997 Umbria-Marche (central Italy) seismic sequence: Geophysical Research Letters, v. 32, L10311, https://doi.org/10.1029/2004GL022256.

Bense, V.F., and Person, M.A., 2006, Faults as conduit-barrier systems to fluid flow in siliciclastic sedimentary aquifers: Water Resources Research, v. 42, W05421, https://doi.org/10.1029/2005WR004480.

Brenguier, F., Campillo, M., Takeda, T., Aoki, Y., Shapiro, N.M., Briand, X., Emoto, K., and Miyake, H., 2014, Mapping pressurized volcanic fluids from induced crustal seismic velocity drops: Science, v. 345, p. 80–82, https://doi.org/10.1126/science.1254073.

Chen, Z., Guo, Z., Zhang, M., and Zhang, L., 2012, CO_2 flux estimations of hot springs in the Tengchong Cenozoic volcanic field, Yunnan province, SW China: Acta Petrologica Sinica (Yanshi Xuebao), v. 28, p. 1217–1224 [in Chinese with English abstract].

Cox, S.F., 2016, Injection-driven swarm seismicity and permeability enhancement: Implications for the dynamics of hydrothermal ore systems in high fluid-flux, overpressured faulting regimes—An

invited paper: Economic Geology, v. 111, p. 559–587, https://doi.org/10.2113/econgeo.111.3.559.
De Barros, L., Cappa, F., Deschamps, A., and Dublanchet, P., 2020, Imbricated aseismic slip and fluid diffusion drive a seismic swarm in the Corinth Gulf, Greece: Geophysical Research Letters, v. 47, https://doi.org/10.1029/2020GL087142.
Dempsey, E.D., Holdsworth, R.E., Imber, J., Bistacchi, A., and Di Toro, G., 2014, A geological explanation for intraplate earthquake clustering complexity: The zeolite-bearing fault/fracture networks in the Adamello Massif (Southern Italian Alps): Journal of Structural Geology, v. 66, p. 58–74, https://doi.org/10.1016/j.jsg.2014.04.009.
Deng, Q., Zhang, P., Ran, Y., Yang, X., Min, W., and Chu, Q., 2003, Basic characteristics of active tectonics of China: Science in China Series D: Earth Sciences, v. 46, p. 356–372, https://doi.org/10.1360/03yd9032.
Duan, Y., Wei, Z., Yang, X., Ye, B., and Wang, J., 2019, Research progress and prospect of structure in Tengchong volcanic area: Progress in Geophysics (in Chinese), v. 34, no. 4, p. 1288–1297, https://doi.org10.6038/pg2019CC0219.
Ester, M., Kriegel, H.-P., Sander, J., and Xu, X., 1996, A density-based algorithm for discovering clusters in large spatial databases with noise, *in* Simoudis, E., et al., eds., KDD'96: Proceedings of the Second International Conference on Knowledge Discovery and Data Mining: Association for the Advancement of Artificial Intelligence Press, p. 226–231.
Guglielmi, Y., Cappa, F., Avouac, J.-P., Henry, P., and Elsworth, D., 2015, Seismicity triggered by fluid injection–induced aseismic slip: Science, v. 348, p. 1224–1226, https://doi.org/10.1126/science.aab0476.
Guo, Q., Planer-Friedrich, B., Liu, M., Li, J., Zhou, C., and Wang, Y., 2017, Arsenic and thioarsenic species in the hot springs of the Rehai magmatic geothermal system, Tengchong volcanic region, China: Chemical Geology, v. 453, p. 12–20, https://doi.org/10.1016/j.chemgeo.2017.02.010.
Hildreth, W., and Fierstein, J., 2012, The Novarupta-Katmai eruption of 1912—Largest eruption of the twentieth century: Centennial perspectives. U.S. Geological Survey Professional Paper 1791, 244 p., https://doi.org/10.3133/pp1791.
Hill, D.P., 1977, A model for earthquake swarms: Journal of Geophysical Research, v. 82, p. 1347–1352, https://doi.org/10.1029/JB082i008p01347.
Hu, S., He, L., and Wang, J., 2000, Heat flow in the continental area of China: A new data set: Earth and Planetary Science Letters, v. 179, p. 407–419, https://doi.org/10.1016/S0012-821X(00)00126-6.
Kim, T., and Avouac, J.-P., 2023, Stress-based and convolutional forecasting of injection-induced seismicity: Application to the Otaniemi geothermal reservoir stimulation: Journal of Geophysical Research: Solid Earth, v. 128, https://doi.org/10.1029/2022JB024960.
Li, Y., Shan, X., Gao, Z., and Huang, X., 2023, Interseismic coupling, asperity distribution, and earthquake potential on major faults in southeastern Tibet: Geophysical Research Letters, v. 50, https://doi.org/10.1029/2022GL101209.
Liu, M., Li, L., Zhang, M., Lei, X., Nedimovic, M.R., Plourde, A.P., Guo, R., Wang, W., and Li, H., 2023, Complexity of initiation and evolution of the 2013 Yunlong earthquake swarm: Earth and Planetary Science Letters, v. 612, https://doi.org/10.1016/j.epsl.2023.118168.
Mogi, K., 1963, Some discussions on aftershocks, foreshocks and earthquake swarms—The fracture of a semi-infinite body caused by an inner stress origin and its relation to the earthquake phenomena (third paper): Bulletin of the Earthquake Research Institute, v. 41, p. 615–658.
Parotidis, M., Shapiro, S.A., and Rothert, E., 2004, Back front of seismicity induced after termination of borehole fluid injection: Geophysical Research Letters, v. 31, L02612, https://doi.org/10.1029/2003GL018987.
Patrick, M.R., Houghton, B.F., Anderson, K.R., Poland, M.P., Montgomery-Brown, E., Johanson, I., Thelen, W., and Elias, T., 2020, The cascading origin of the 2018 Kīlauea eruption and implications for future forecasting: Nature Communications, v. 11, 5646, https://doi.org/10.1038/s41467-020-19190-1.
Peng, G., Lei, X., Wang, G., and Jiang, F., 2021, Precursory tidal triggering and *b* value variation before the 2011 M_w 5.1 and 5.0 Tengchong, China earthquakes: Earth and Planetary Science Letters, v. 574, https://doi.org/10.1016/j.epsl.2021.117167.
Ross, Z.E., and Cochran, E.S., 2021, Evidence for latent crustal fluid injection transients in Southern California from long-duration earthquake swarms: Geophysical Research Letters, v. 48, https://doi.org/10.1029/2021GL092465.
Scholz, C.H., 2019, The Mechanics of Earthquakes and Faulting (3rd edition): Cambridge, UK, Cambridge University Press, 512 p., https://doi.org/10.1017/9781316681473.
Shangguan, Z., Zhao, C., Li, H., Gao, Q., and Sun, M., 2005, Evolution of hydrothermal explosions at Rehai geothermal field, Tengchong volcanic region, China: Geothermics, v. 34, p. 518–526, https://doi.org/10.1016/j.geothermics.2005.05.002.
Shapiro, S.A., Huenges, E., and Borm, G., 1997, Estimating the crust permeability from fluid injection-induced seismic emission at the KTB site: Geophysical Journal International, v. 131, p. F15–F18, https://doi.org/10.1111/j.1365-246X.1997.tb01215.x.
Shelly, D.R., Hill, D.P., Massin, F., Farrell, J., Smith, R.B., and Taira, T., 2013, A fluid-driven earthquake swarm on the margin of the Yellowstone caldera: Journal of Geophysical Research: Solid Earth, v. 118, p. 4872–4886, https://doi.org/10.1002/jgrb.50362.
Sibson, R.H., 1981, Fluid flow accompanying faulting: Field evidence and models, *in* Simpson, D.W., and Richards, P.G., eds., Earthquake Prediction: An International Review: American Geophysical Union Maurice Ewing Series 4, p. 593–603, https://doi.org/10.1029/ME004p0593.
Tapponnier, P., Peltzer, G., Le Dain, A.Y., Armijo, R., and Cobbold, P., 1982, Propagating extrusion tectonics in Asia: New insights from simple experiments with plasticine: Geology, v. 10, p. 611–616, https://doi.org/10.1130/0091-7613(1982)10<611:PETIAN>2.0.CO;2.
Vidale, J.E., and Shearer, P.M., 2006, A survey of 71 earthquake bursts across southern California: Exploring the role of pore fluid pressure fluctuations and aseismic slip as drivers: Journal of Geophysical Research, v. 111, B05312, https://doi.org/10.1029/2005JB004034.
Wells, D.L., and Coppersmith, K.J., 1994, New empirical relationships among magnitude, rupture length, rupture width, rupture area, and surface displacement: Bulletin of the Seismological Society of America, v. 84, p. 974–1002, https://doi.org/10.1785/BSSA0840040974.
Wilding, J.D., Zhu, W., Ross, Z.E., and Jackson, J.M., 2023, The magmatic web beneath Hawai'i: Science, v. 379, p. 462–468, https://doi.org/10.1126/science.ade5755.
Ye, T., Huang, Q., Chen, X., Zhang, H., Chen, Y.J., Zhao, L., and Zhang, Y., 2018, Magma chamber and crustal channel flow structures in the Tengchong volcano area from 3-D MT inversion at the intracontinental block boundary southeast of the Tibetan Plateau: Journal of Geophysical Research: Solid Earth, v. 123, p. 11,112–11,126, https://doi.org/10.1029/2018JB015936.

Printed in the USA

Liu, M., et al., 2024, Intersection between tectonic faults and magmatic systems promotes swarms with large-magnitude earthquakes around the Tengchong volcanic field, southeastern Tibetan Plateau: Geology, https://doi.org/10.1130/G51796.1

Supplemental Material

Seismic data processing procedure and high-resolution earthquake catalog.

Supplementary materials for

Intersection between tectonic faults and magmatic systems promotes swarms with large-magnitude earthquakes around the Tengchong volcanic field, southeastern Tibetan Plateau

Min Liu[1, 2], Yen Joe Tan[1*], Xinglin Lei[3], Hongyi Li[2], Yunpeng Zhang[4], Weitao Wang[4]

[1]Earth and Environmental Sciences Programme, Faculty of Science, The Chinese University of Hong Kong, Hong Kong, China, 999073

[2]Key Laboratory of Intraplate Volcanoes and Earthquakes, Ministry of Education, China University of Geosciences (Beijing), Beijing, China, 100083

[3]National Institute of Advanced Industrial Science and Technology, Tsukuba, Japan, 305-8567

[4]Institute of Geophysics, China Earthquake Administration, Beijing, China, 100036

*Corresponding author. Email: yjtan@cuhk.edu.hk

Contents of this file

Introduction

This supporting information provides eight texts and nine figures to support the discussions in the main text.

Text S1: Machine learning-based phase picking and association

Routine catalogs in the Yunnan province usually have low resolution due to the sparse permanent seismic network (Liu et al., 2022b, 2023). Here, we first develop a high-resolution catalog using continuous seismic data from both the permanent (2009 to 2022) and temporary (2011 to 2013) seismic network, which in total include 19 broadband seismometers with a 100 Hz sampling rate. The data processing procedure mainly follows the machine-learning-based workflow implemented by Liu et al. (2023). We first use LPPN, a lightweight network-based phase picker (Yu & Wang, 2022), to identify P- and S-wave arrival times from the continuous waveforms. LPPN outputs a probability value for each pick to quantify the picking quality. We only keep P- and S-wave arrival times with at least a 0.3 probability value to remove possible false picks. Subsequently, these remaining P- and S-wave arrival times are associated into individual earthquakes using a Bayesian Gaussian Mixture model (GaMMA; Zhu et al., 2022). A strict threshold of three P picks, three S picks and a total of eight P and S picks is adopted during the GaMMA association, resulting in 60,099 earthquakes within a region of 1° × 1° (latitude: 24.6° to 25.6°; longitude: 97.8° to 98.8°) from 2009 to 2022.

Text S2: Earthquake relocation

We use a sequential location procedure to refine 19,954 hypocenters around the TVF (latitude: 24.7° to 25.3°; longitude: 98.25° to 98.80°) with good station coverage. We first utilize a non-linear oct-tree grid-search algorithm (NonLinLoc) with a 1-D velocity model to update the absolute locations of the 19,954 earthquakes (Lomax et al., 2000). Among them, we select 18,772 earthquakes with a station gap of < 200° and travel time residual of < 0.6 seconds, to further refine their hypocenters based on their catalog differential arrival times using the relative location method hypoDD (Waldhauser & Ellsworth, 2000). The probabilities of the picks obtained from LPPN are used as phase weighting in hypoDD. The maximum separation and minimum links of event pairs are 10 km and 8, respectively. We successfully relocate 17,747 earthquakes. Subsequently, we

utilize a waveform cross-correlation-based relative location method GrowClust to relocate the 17,747 earthquakes (Trugman & Shearer, 2017). We first build an event-pair database using the ph2dt program provided by the hypoDD software package (Waldhauser & Ellsworth, 2000). Each earthquake is paired with other events within < 5 km. The minimum links and maximum distance from the station for each event-pair are defined as 8 and 120 km, respectively. We then implement the fast double-difference cross-correlation algorithm (FDTCC) to measure the cross-correlation differential times for all event-pairs (Liu et al., 2023). All event waveforms are filtered from 1 to 12 Hz. The window lengths of P- and S-waves are defined as 3 and 4 seconds respectively, starting 0.25 seconds before the LPPN-picked arrival times. When the LPPN-based picks are unavailable, we use the TauP toolkit to predict the arrivals based on a 1-D velocity model (Crotwell et al., 1999). In GrowClust, the minimum correlation coefficient threshold and the number of differential times per event-pair for relocation are defined as 0.7 and 8, respectively. We successfully relocate 10,078 earthquakes (Figure 1). We further perform a bootstrapping analysis using GrowClust to estimate the relative location uncertainty for all relocated events. The mean horizontal and vertical uncertainties are 54 m and 147 m, respectively.

Text S3: Relocating the hypocenters of the three largest events

Due to rupture complexity, the three largest events could not be paired with other smaller events based on FDTCC. We thus adopt a GPU-based Match&Locate method (GPU-M&L) to determine their initial rupture points based on their initial P waves (Liu et al., 2020, 2022a). We first select three reference events with clear P-wave first motions from our relocated catalog. The template length is defined as 0.15 s starting 0.1 s before the manually picked P-wave arrivals, whereas the waveform windows of the three target events are 5 s before and 50 s after their origin times. To improve the spatial resolution, we further interpolate the template and target waveforms from 100 to 5000 Hz in the frequency domain (Liu et al., 2022a). Finally, based on a grid-search strategy, GPU-M&L determines the initial rupture points of the three largest events by maximizing the cross-correlation coefficients between template windows and target waveform segments (Liu et al., 2020, 2022a).

Text S4: Magnitude estimation

We estimate the local magnitudes for all relocated earthquakes based on their S-wave amplitudes and a recently improved national standard magnitude scale that is specific to the Yunnan region, China (Richter, 1935; Lin et al., 2018). The maximum amplitudes of horizontal component waveforms are measured after deconvolving the instrument response from the raw waveforms and then convolving the obtained signal with the theoretical Wood-Anderson seismometer response. The measured waveform window starts 0.5 seconds before the P wave arrival and is twice the predicted S–P travel time in length. The estimated magnitudes range from M_L 0.02 to 5.20 with a completeness magnitude of 0.8 (Figure S9).

Text S5: Earthquake swarm identification

We systematically detect potential earthquake swarms from our newly developed catalog. Based on 3D earthquake hypocenters, we initially identified 664 earthquake clusters using the DBSCAN algorithm (Ester et al., 1996) with the sphere radius and minimum number of points defined as 0.5 km and 1, respectively. Eleven clusters with at least 100 events are then selected for manual inspection where we only keep burst-like clusters and exclude those typical mainshock-aftershock sequences with the largest events occurring towards the beginning of the sequence. This leaves us with five earthquake swarms containing 5,905 events (Figures S1-S2).

Text S6: Rupture dimension estimation

Rupture dimensions of the main events in swarms 2 and 4 are estimated based on Wells & Coppersmith (1994). Pang et al. (2021) used the gCAP method to calculate the moment magnitudes of the two M_L 5.2 main events in swarm 5, which are Mw 5.1 and 5.0, respectively. It suggests that the moment magnitude of an earthquake in Tengchong is lower than its local magnitude. Since an Mw 4.7 earthquake can rupture a length of ~1.5 km, we infer that the actual rupture dimensions of the two main events (M_L 4.6 and 4.7) in swarms 2 and 4 are both likely less than ~1.5 km.

Text S7: Focal mechanism solutions

We use HASH to obtain the focal mechanism solutions for the first M_L 4.7 main event and nine $M_L > 2.5$ events that occurred on the ring-like fault based on P-wave first motions and S/P amplitude ratios (Hardebeck and Shearer, 2002, 2003). Results show that these earthquakes are predominately strike-slip and normal faulting events (Figures 3, S4 and S5). These earthquakes

that occurred within the ring-like structure exhibit rotated nodal planes (Figure S5). Since the amplitudes of the two M_L 5.2 main events exceed the dynamic range of seismometers used in this study, we thus obtain their focal mechanism solutions from a previous study which applied the generalized cut and paste method using data from seismometers located farther away (Peng et al., 2021). Both M_L 5.2 events are strike-slip events (Figure 3).

Text S8: Regional stress field inversion

We first collect the focal mechanism solutions of 20 $M_W > 5.3$ earthquakes that occurred around TVF (latitude: 20° to 25°; longitude: 97° to 102°) between 1976 and 2021 from the Global Centroid Moment Tensor catalog (https://www.globalcmt.org/CMTsearch.html). We then use a damped linear inversion technique to invert the regional stress field based on these earthquakes (Hardebeck and Michael, 2006). Results show that the greatest principal stress is nearly horizontal (plunge = 1.7°, standard error = 8°) with an azimuth angle of ~10° and the stress shape ratio is ~0.5 (Figure S8), which is conducive for the formation of strike-slip faults with strike directions of ~40° and ~340° (e.g., Yu et al., 2022).

References:

1. Crotwell, H. P., Owens, T. J., Ritsema, J., et al. (1999). The taup toolkit: Flexible seismic travel-time and ray-path utilities. Seismological Research Letters, 70, 154–160.
2. Ester, M., Kriegel, H. P., Sander, J., Xu, X., et al. (1996). A density-based algorithm for discovering clusters in large spatial databases with noise., in: kdd, pp. 226–231.
3. Hardebeck, J. L. & Michael, A. J. (2006). Damped regional-scale stress inversions: Methodology and examples for southern california and the coalinga aftershock sequence. Journal of Geophysical Research: Solid Earth, 111.
4. Hardebeck, J. L. & Shearer, P. M. (2002). A new method for determining first motion focal mechanisms. Bulletin of the Seismological Society of America, 92, 2264–2276.
5. Hardebeck, J. L. & Shearer, P. M. (2003). Using s/p amplitude ratios to constrain the focal mechanisms of small earthquakes. Bulletin of the Seismological Society of America, 93, 2434–2444.

6. Liu, M., Li, H., Zhang, M. & Wang, T. (2020). Graphics processing unit-based match and locate (GPU-M&L): An improved match and locate method and its application. Seismological Research Letters, 91, 1019–1029.

7. Liu, M., Zhang, M. & Li, H. (2022a). Using the match-and-locate method to characterize foreshocks of the July 2019 Mw6. 4 Ridgecrest, California earthquake. Earthquake Science, 35, 213–242.

8. Liu, M., Li, H., Li, L., Zhang, M. & Wang, W. (2022b). Multistage nucleation of the 2021 Yangbi Ms 6.4 earthquake, Yunnan, China and its foreshocks. Journal of Geophysical Research: Solid Earth, 127, e2022JB024091.434

9. Liu, M., Li, L., Zhang, M., Lei, X., Nedimović, M.R., Plourde, A.P., Guo, R., Wang, W. & Li, H. (2023). Complexity of initiation and evolution of the 2013 Yunlong earthquake swarm. Earth and Planetary Science Letters, 612, 118168.

10. Lomax, A., Virieux, J., Volant, P. & Berge-Thierry, C. (2000). Probabilistic earthquake location in 3d and layered models: Introduction of a metropolis-gibbs method and comparison with linear locations. Advances in seismic event location, 101–134.

11. Omori, F., 1895. On the after-shocks of earthquakes. Ph.D. thesis. The University of Tokyo.

12. Peng, G., Lei, X., Wang, G., & Jiang, F. (2021). Precursory tidal triggering and b value variation before the 2011 Mw 5.1 and 5.0 Tengchong, china earthquakes. Earth and Planetary Science Letters, 574 , 117167.

13. Richter, C. F. (1935). An instrumental earthquake magnitude scale. Bulletin of the seismological society of America, 25, 1–32.

14. Tang, L., Qi, G., Su, J., Huang, Chunmei, Fu, Y. & Yan, L. (2018). Comparison of the new national standard magnitude scales with the traditional magnitude scales. Acta Seismologica Sinica, 40, 121–131.

15. Trugman, D. T. & Shearer, P. M. (2017). Growclust: A hierarchical clustering algorithm for relative earthquake relocation, with application to the spanish springs and sheldon, Nevada, earthquake sequences. Seismological Research Letters, 88, 379–391.

16. Yu, H., Kao, H., Wang, B. & Visser, R. (2022). Long-term fluid injection can expedite fault reactivation and development: Riedel shear structures illuminated by induced earthquakes in Alberta, Canada. Journal of Geophysical Research: Solid Earth, 127, e2022JB0251

17. Yu, Z. & Wang, W. (2022). Lppn: A lightweight network for fast phase picking. Seismological Society of America, 93, 2834–2846.

18. Zhu, W., McBrearty, I. W., Mousavi, S. M., Ellsworth, W. L. & Beroza, G. C. (2022). Earthquake phase association using a bayesian gaussian mixture model. Journal of Geophysical Research: Solid Earth, 127, e2021JB023249.

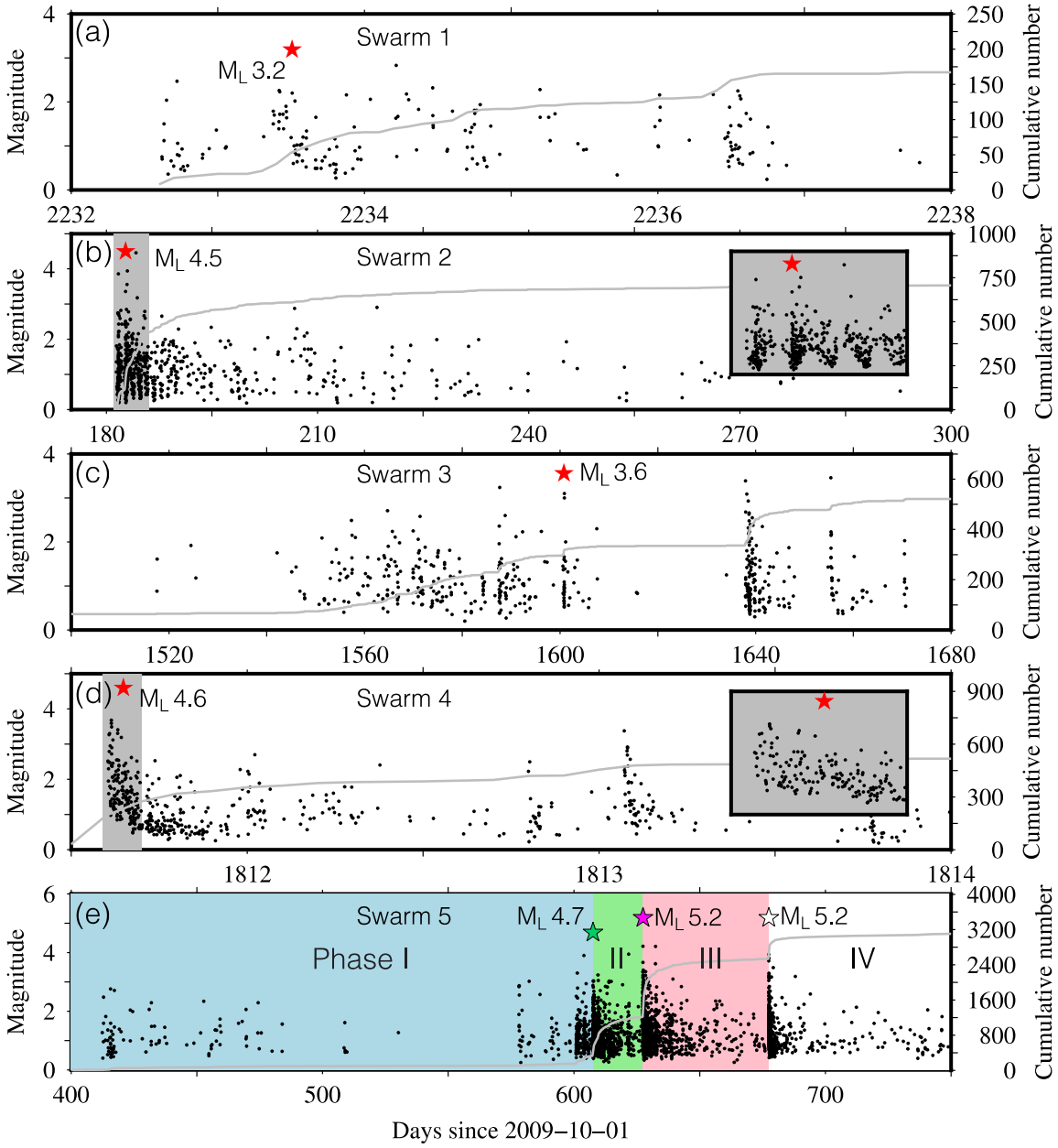

Figure S1. Magnitude-time evolution of earthquake swarms. Red stars in (a-d) represent the largest events in swarms 1-4. Gray lines in (a-e) indicate the cumulative number of events with time. Insets in (b) and (d) show the zoom-in time periods, which are marked by gray rectangles. Three colored stars in (e) indicate the three largest events dividing swarm 5 into four episodes.

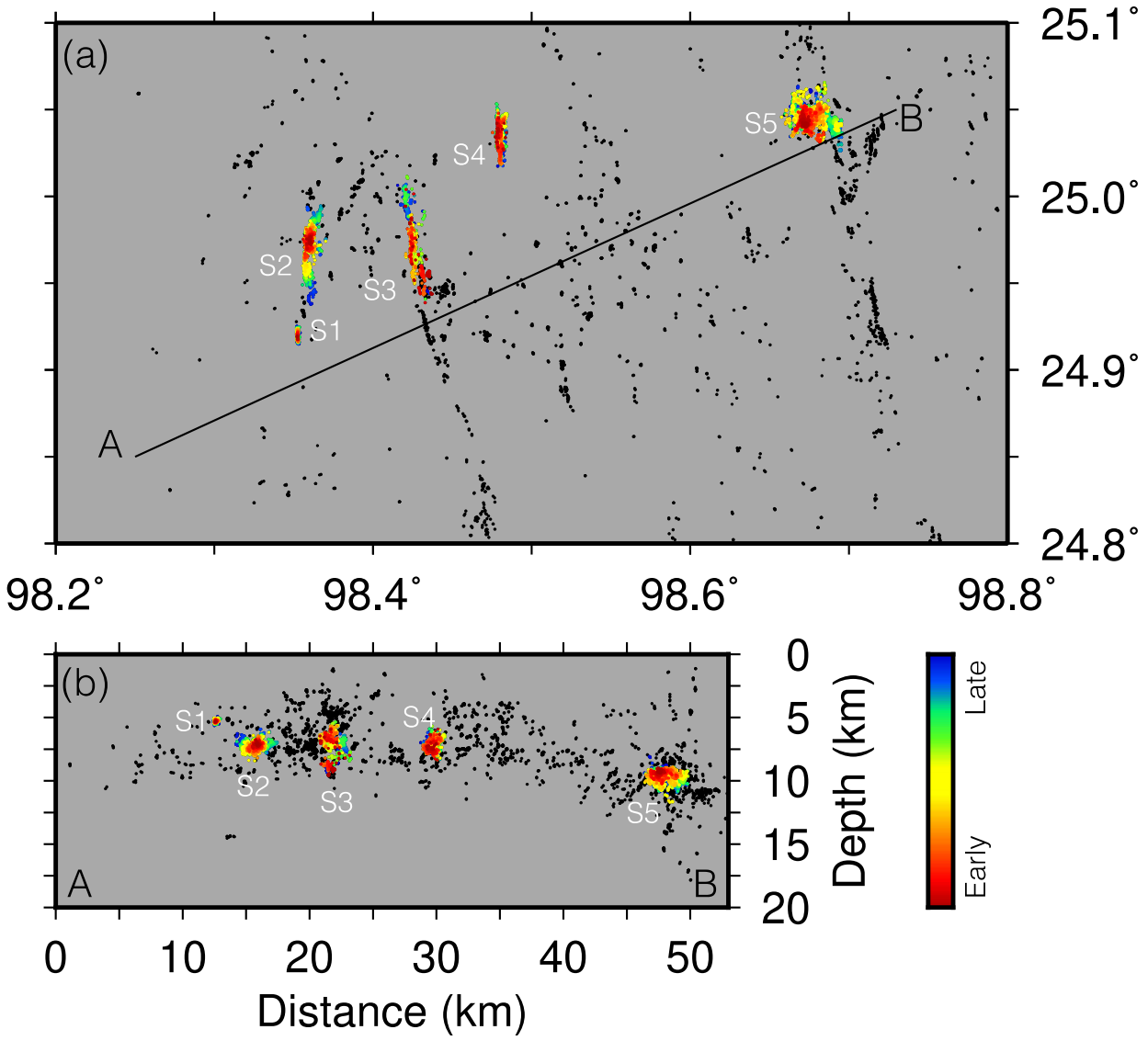

Figure S2. Similar to Figure 1b-c, but with color indicating the origin time of the identified swarms.

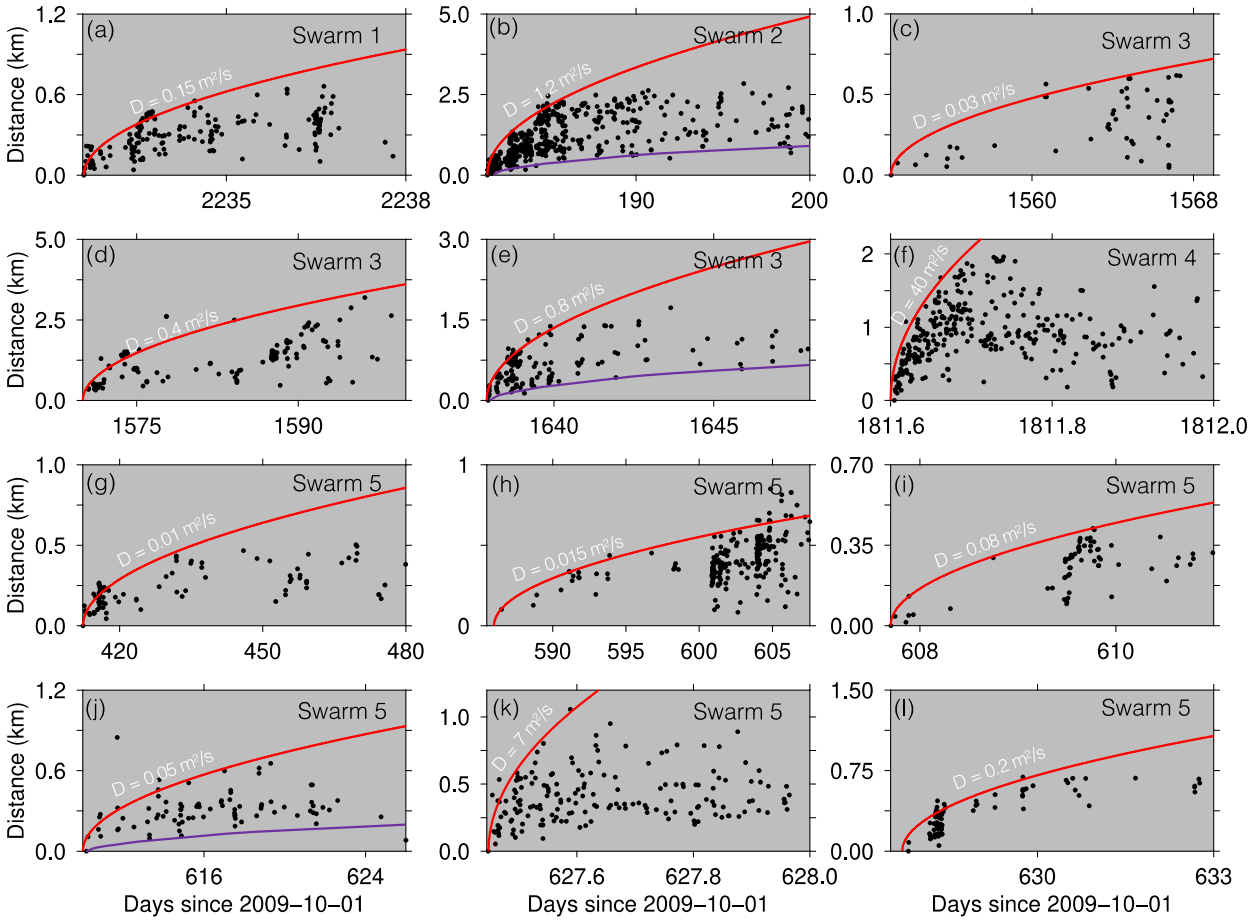

Figure S3. Distance from the initiation points with time. Red curves represent the best-fit fluid diffusion models. Purple curves indicate the possible back fronts of fluid diffusion.

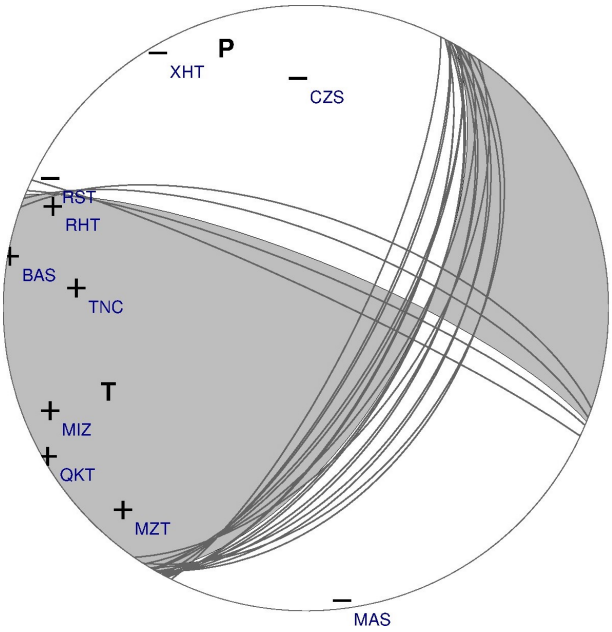

2011–05–31 13:13:36
ID: 20110531131336
Lat.: 25.042°N
Lon.: –98.670°E
Dep.: 10 km
Str, Dip, Rake: 292 77 150
RMS: 8

Figure S4. Focal mechanism solution of the first main ML 4.7 event solved based on P-wave first motions (+, up; –, down) and S/P amplitude ratios.

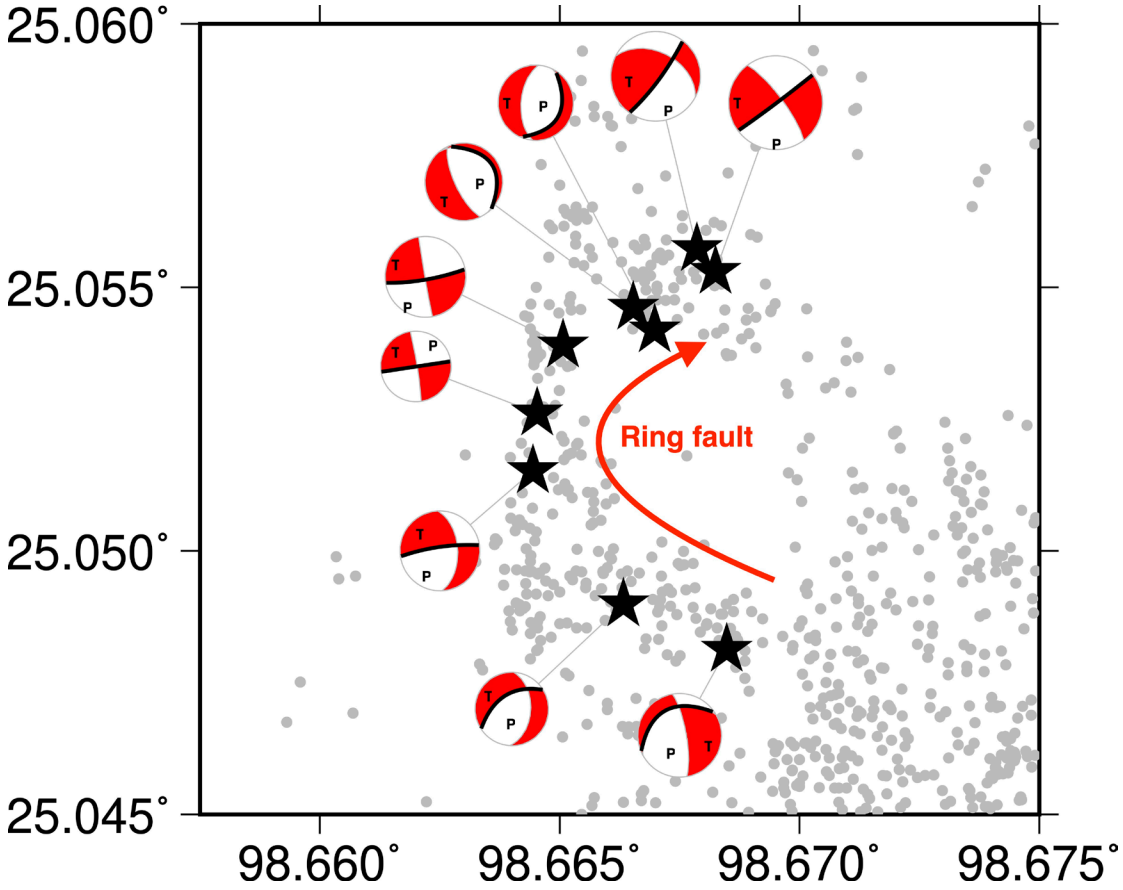

Figure S5. Illuminating the ring-like structure through the focal mechanisms of nine relatively large events. Clear rotation of nodal planes (black curves) is exhibited in this panel.

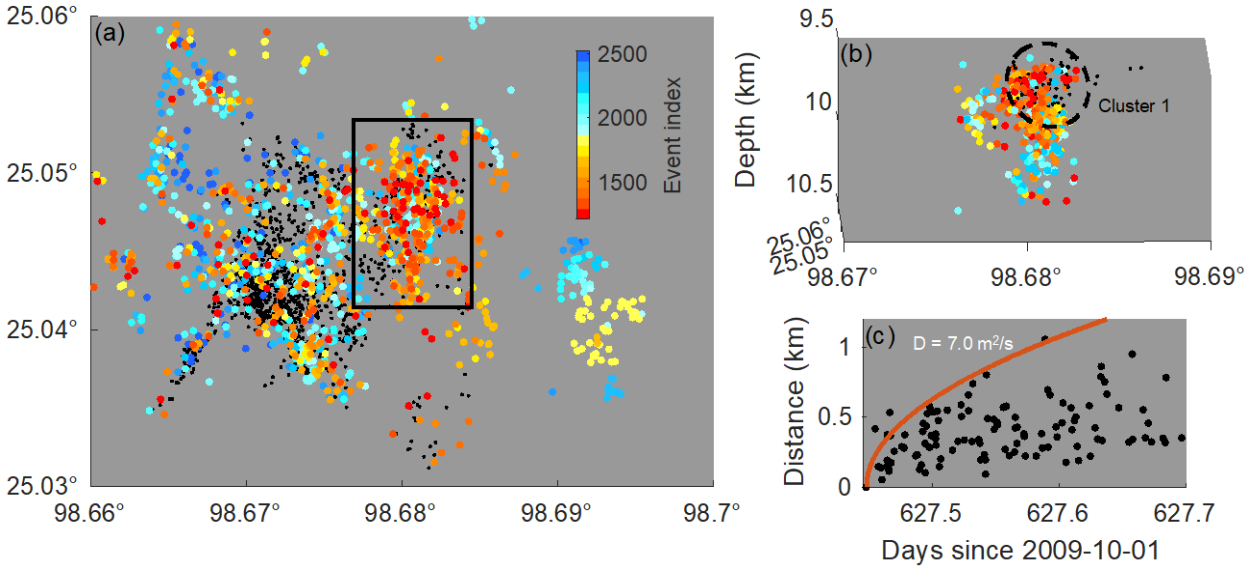

Figure S6. Spatiotemporal evolution of phase 3 of swarm 5. (a) Map view of the earthquakes that occurred during phase 3 with color indicating event index. Black rectangle marks a fluid-driven sub-swarm with a zoom-in 3D view and migration front exhibited in (b) and (c), respectively. Black dashed circle in (b) indicates cluster 1. Red curve in (c) represents the fluid diffusion model with a diffusivity of 7.0 m^2/s.

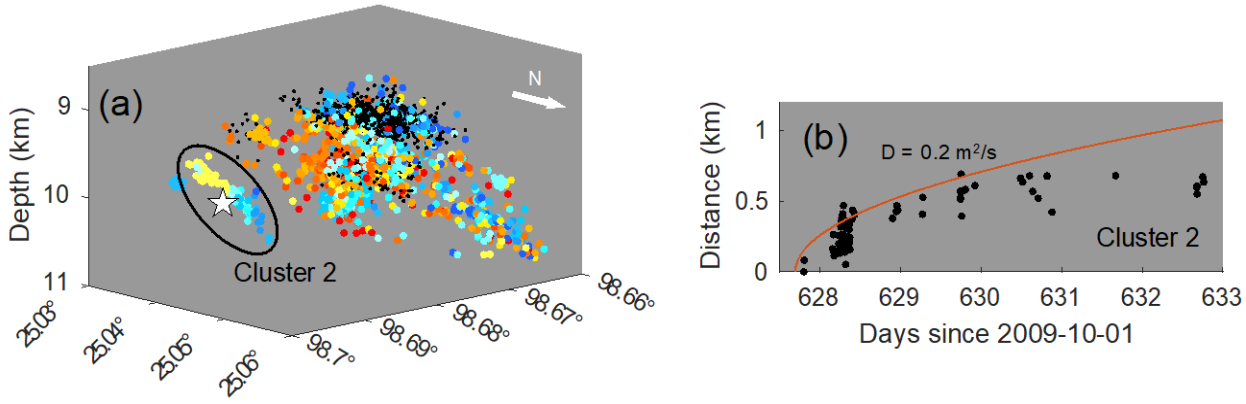

Figure S7. (a) 3D view of the isolated cluster 2. (b) Migration front of earthquakes that occurred within the isolated cluster 2, which can be well-fitted by the fluid diffusion model (red curve).

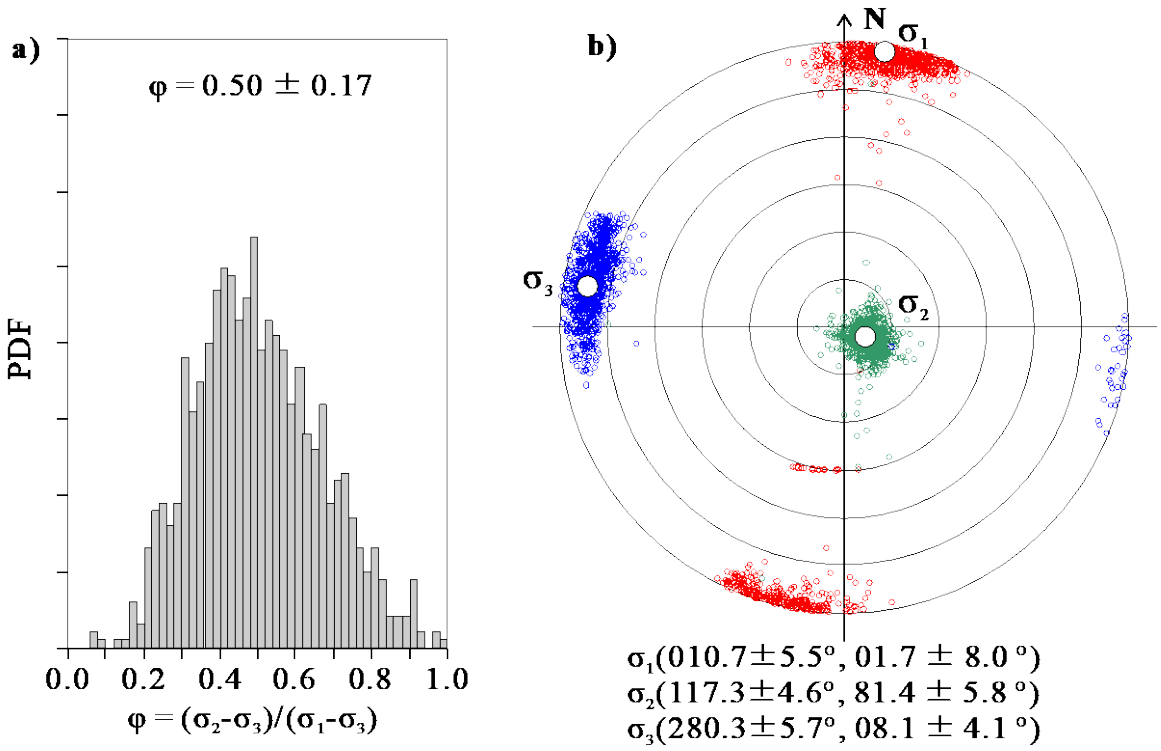

Figure S8. Regional stress field inversion. (a) Estimated stress shape ratio of the principal stresses. (b) Estimated azimuths and dip angles of the principal stresses with errors.

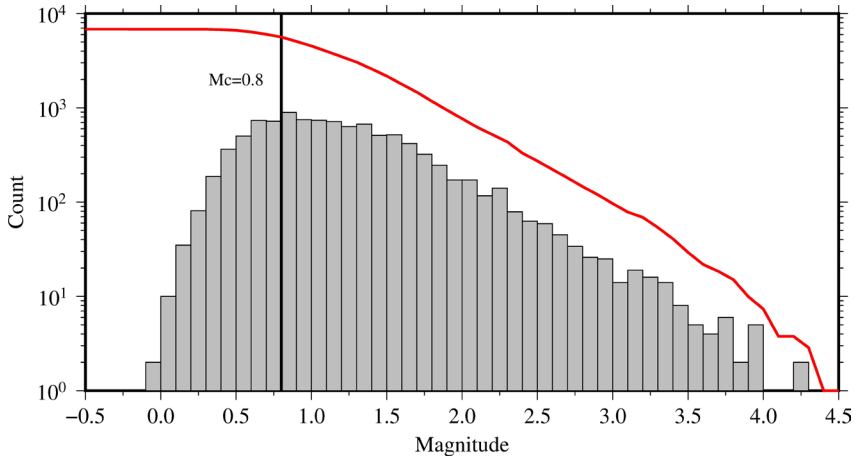

Figure S9. Frequency-magnitude distribution and magnitude of completeness (Mc) of our newly developed catalog.